

Pseudogap Formation and Heavy Carrier Dynamics in Intermediate Valence YbAl<sub>3</sub>Hidekazu OKAMURA\*, Takahiro MICHIZAWA, Takao NANBA and Takao EBIHARA<sup>1</sup>*Graduate School of Science and Technology, Kobe University, Kobe 657-8501.*<sup>1</sup>*Department of Physics, Shizuoka University, Shizuoka 422-8529.*

(Received September 16, 2018)

Infrared optical conductivity [ $\sigma(\omega)$ ] of the intermediate valence compound YbAl<sub>3</sub> has been measured at temperatures  $8 \text{ K} \leq T \leq 690 \text{ K}$  to study its microscopic electronic structures. Despite the highly metallic characters of YbAl<sub>3</sub>,  $\sigma(\omega)$  exhibits a clear pseudogap (strong depletion of spectral weight) of about 60 meV below 40 K. It also shows a strong mid-infrared peak centered at  $\sim 0.25 \text{ eV}$ . Energy-dependent effective mass and scattering rate of the carriers obtained from the data indicate the formation of a heavy-mass Fermi liquid state. These characteristic results are discussed in terms of the hybridization states between the Yb 4*f* and the conduction electrons. It is argued, in particular, that the pseudogap and the mid-infrared peak result from the indirect and the direct gaps, respectively, within the hybridization state.

KEYWORDS: YbAl<sub>3</sub>, strongly correlated electron system, intermediate valence, heavy fermion, optical conductivity

The duality and crossover between localized and itinerant characters exhibited by the 4*f* electrons in rare-earth compounds, most typically those containing a lattice of Ce or Yb ions, has been a central issue in the physics of strongly correlated electron systems.<sup>1</sup> Such duality results from a hybridization of conduction (*c*) electrons having spatially extended wave functions and *f* electrons having localized orbitals. At temperatures  $T \simeq T_K$ , where  $T_K$  is the single-site Kondo temperature, the *f* electrons are localized well at each site. The Kondo effect at individual sites give rise to a  $\rho_m \propto -\log T$  behavior, where  $\rho_m(T)$  is the magnetic contribution to the resistivity. In contrast, below another characteristic temperature  $T^*$ , where  $T^* \ll T_K$  in general, the *f* electrons become partly itinerant as a “heavy quasiparticle band” is formed. This is a spatially extended state consisting of both *c* and *f* electron wave functions with large effective masses ( $m^*$ ), which shows Fermi liquid properties such as  $\rho_m \propto T^2$  dependence below  $T^*$ . ( $T^*$  is sometimes referred to as the coherence temperature.) The magnetic susceptibility,  $\chi(T)$ , shows a maximum at  $T = T_{max}$ , marking a crossover between the local moment (Curie Weiss) regime above  $T_{max}$  and the free carrier (Pauli paramagnetism) regime below  $T_{max}$ . The values of  $m^*$  and  $T_{max}$  are measures of the hybridization strength. “Heavy fermion” (HF) compounds have only a weak hybridization, and show large  $m^*$  values (up to  $\sim 1000 m_0$ ) and  $T_{max}$  of typically a few K or lower. In contrast, “intermediate valence” (IV) compounds have a stronger hybridization, showing typically  $m^* = 10\text{-}100 m_0$ ,  $T_{max} = 20\text{-}300 \text{ K}$ , and the Ce or Yb valence away from 3+. In addition to the metallic cases described above, there are a small number of “Kondo semiconductors”, where the *c-f* hybridization leads to semiconducting characteristics.<sup>3,4</sup>

Although the above scenario is generally accepted, the microscopic mechanism for the *c-f* hybridization and its consequences are not yet precisely known. Optical conductivity technique has emerged as a powerful tool for

studying the microscopic electronic structures in *f* electron systems.<sup>5</sup> It has been applied to many HF and IV compounds, including metals (CeCu<sub>6</sub>,<sup>5</sup> CePd<sub>3</sub><sup>6</sup>), Kondo semiconductors (SmB<sub>6</sub>,<sup>7</sup> Ce<sub>3</sub>Bi<sub>4</sub>Pt<sub>3</sub>,<sup>8</sup> YbB<sub>12</sub><sup>9,10</sup>), and more recently filled-skutterudite compounds.<sup>11,12</sup>

In this work we have applied the optical technique to YbAl<sub>3</sub>, which is a well-known IV compound extensively studied for the last few decades. Recently, the first observation of the de Haas-van Alphen (dHvA) effect in YbAl<sub>3</sub> was reported,<sup>13,14</sup> and YbAl<sub>3</sub> is gaining renewed interest.<sup>15-17</sup> The  $m^*$  values obtained by dHvA are 14-24  $m_0$ , the specific heat coefficient is  $\gamma \sim 40 \text{ mJ/mol}\cdot\text{K}^2$ ,  $T^* \sim 35 \text{ K}$  and  $T_{max} \sim 120 \text{ K}$ . Experimentally estimated single-site  $T_K$  and the Yb mean valence are in the ranges 600-700 K (50-60 meV) and 2.7-2.8, respectively.<sup>15,18</sup> These results suggest a rather strong *c-f* hybridization in YbAl<sub>3</sub>. The measured optical conductivity spectrum  $\sigma(\omega)$  of YbAl<sub>3</sub> has shown strong *T* dependences,<sup>21</sup> which are analyzed based on the *c-f* hybridization scenario within the framework of the periodic Anderson model.

YbAl<sub>3</sub> single crystals used in this work were grown with a self-flux method.<sup>13</sup> Samples taken from the same batch showed clear dHvA oscillations, indicating a high quality.  $\sigma(\omega)$  spectra were obtained from the measured optical reflectivity spectra  $R(\omega)$  using the Kramers-Kronig relations.<sup>20</sup>  $R(\omega)$  was measured in the range 7 meV - 35 eV on mechanically polished surfaces of the samples, under a near-normal incidence using a thermal source and a synchrotron radiation source at BL7B of the UVSOR, Institute for Molecular Science. A gold or a silver film deposited *in situ* onto the sample surface was used as a reference of the reflectivity.<sup>19</sup> To complete  $R(\omega)$ , a Hagen-Rubens formula was used for low-energy extrapolation,<sup>20</sup> and an  $\omega^{-4}$  function for high-energy extrapolation.

Figure 1(a) shows  $R(\omega)$  of YbAl<sub>3</sub> at 295 K in the entire measured energy range, and Figure 1(b) shows the low-energy part of  $R(\omega)$  at  $8 \text{ K} \leq T \leq 690 \text{ K}$  and that of

\*E-mail: okamura@phys.sci.kobe-u.ac.jp

non-magnetic  $\text{LuAl}_3$  at 295 K.  $\text{YbAl}_3$  has a broad dip in  $R(\omega)$  below 0.5 eV, which becomes more pronounced with decreasing  $T$ . In contrast,  $\text{LuAl}_3$  has no such feature in  $R(\omega)$ . These results indicate that the dip in  $R(\omega)$  of  $\text{YbAl}_3$  is caused by the Yb  $4f$ -related electronic states located near the Fermi level ( $E_F$ ).

Figure 2(a) shows  $\sigma(\omega)$  of  $\text{YbAl}_3$  over a wide energy range for  $8 \text{ K} \leq T \leq 690 \text{ K}$ , and Fig. 2(b) shows those in the infrared region below 295 K.  $\sigma(\omega)$  spectra are characterized by the following three key features, all of which are strongly  $T$ -dependent: First, a steep rise of  $\sigma(\omega)$  toward  $\omega=0$  is observed. This is due to the Drude response of free carriers.<sup>20</sup> Second, a pronounced mid-infrared (mIR) peak centered near 0.25 eV is observed, which becomes gradually stronger with decreasing  $T$ . This peak results from the dip in  $R(\omega)$  discussed above, and shows the existence of strong excitations due to the Yb  $4f$ -derived electronic states near  $E_F$ . The third feature is the appearance below 120 K of a strong depletion (pseudogap) of  $\sigma(\omega)$ , indicated by the vertical arrow in Fig. 2(b), and the associated shoulder at 60 meV, indicated by the vertical broken line. The pseudogap formation in  $\sigma(\omega)$  evidences that the density of states (DOS) near  $E_F$  decreases below 120 K. Note that  $T_{max}$  of  $\text{YbAl}_3$  is also 120 K, i.e., the crossover from local moment to free carrier magnetism is coincident with the appearance of the pseudogap and shoulder in  $\sigma(\omega)$ . In addition, the shoulder position (60 meV) agrees well with  $T_K$  of  $\text{YbAl}_3$ .  $\sigma(\omega)$  shows large variation with  $T$  above 40 K, but much less variation between 8 and 40 K. This is explicitly shown Fig. 2(c), which plots  $\sigma(\omega)$  at the pseudogap and the integrated intensity of the mIR peak as a function of  $T$ . Namely, the evolution of the electronic structures with cooling is almost complete at 40 K. This is consistent with the Fermi liquid behavior ( $\rho \propto T^2$ ) of  $\text{YbAl}_3$  observed below  $T^* \simeq 35 \text{ K}$ ,<sup>13,14</sup> i.e., the electronic structures do not change very much once a Fermi liquid state is established. The dc conductivity [ $\sigma_{dc}$ ] and the low-energy region of  $\sigma(\omega)$  are compared to each other in Fig. 2(d). With decreasing  $T$ ,  $\sigma(\omega)$  decreases while  $\sigma_{dc}$  increases rapidly. From this plot, it is apparent that an extremely narrow Drude peak grows below the low-energy limit of our measurement, where at 8 K  $\sigma(\omega)$  increases by more than two orders of magnitude within a range of several meV.

Figure 3 shows the energy-dependent effective mass  $m^*(\omega)$  and the scattering rate  $\tau^{-1}(\omega)$  of the carriers, obtained with the ‘‘generalized Drude’’ analysis<sup>22</sup> to the present data. At 8 K,  $\tau^{-1}(\omega)$  approaches zero with decreasing  $\omega$  below  $\sim 40 \text{ meV}$ , with approximately following an  $\omega^2$  dependence. An  $\omega^2$  dependence of the scattering rate is a signature of the Fermi liquid.<sup>23</sup> In contrast,  $\tau^{-1}(\omega)$  does not approach zero as  $\omega \rightarrow 0$  at higher  $T$ 's. This is consistent with the result that another Fermi liquid property of  $\rho(T) \propto T^2$  is observed only below  $\sim 35 \text{ K}$ .<sup>13</sup>  $m^*(\omega)$  below  $\sim 40 \text{ meV}$  becomes large with decreasing  $T$ , reaching about 30 times the bare band mass at 8 K. This value is consistent with the cyclotron masses of 14-24  $m_0$  obtained by the dHvA experiments.<sup>14</sup>

Among the characteristic optical results of  $\text{YbAl}_3$  presented above, the narrow Drude peak and the mIR peak

are not peculiar to  $\text{YbAl}_3$ , but similar features have been widely observed for many HF/IV metals.<sup>5,24</sup> Although less common, pseudogap formation and heavy-mass Fermi liquid properties have been also reported on some HF-IV compounds, including  $\text{CePd}_3$ .<sup>6</sup> However, the present work is a rare case where all of these characteristic features are observed so clearly for a single compound. Note that the pseudogap in  $\sigma(\omega)$  is not merely a tail of the mIR peak but is a distinct feature, since the former appears below 120 K ( $\sim T_{max}$ ) and becomes well developed only at 40 K and below, while the latter is observed up to much higher temperatures. Namely, the evolution of  $\sigma(\omega)$  appear to exhibit two different characteristic temperatures, as well as two different energy scales (the pseudogap below 60 meV and the mIR peak at 0.25 eV). The relation between these two features is never trivial. Below, we first describe how the narrow Drude peak and the mid-IR peak in HF/IV metals have been interpreted based on the periodic Anderson model (PAM). Then we attempt to analyze the relation between the pseudogap and the mIR peak.

PAM has been a most common model to study theoretically the physical properties of HF/IV compounds.<sup>2,5</sup> Since the PAM cannot be solved exactly, various approximate solutions of PAM have been reported,<sup>4</sup> including explicit calculations of the  $T$ -dependent  $\sigma(\omega)$  based on the dynamical mean field theory.<sup>26-29</sup> According to them, the electronic structures around  $E_F$  at  $T \ll T_K$  can be described by a pair of  $c$ - $f$  hybridized bands, with an associated energy gap, as illustrated in Fig. 4(a). The flatness of the bands near  $E_F$  (large  $m^*$ ) results from the localized character of the (bare)  $f$  electrons. For HF/IV metals,  $E_F$  is located outside the gap. The resulting  $f$ -like, heavy quasiparticles can lead to a narrow Drude peak and Fermi liquid properties such as  $\rho \propto T^2$  and  $1/\tau \propto \omega^2$ .<sup>25</sup> A semiconductor case is realized when  $E_F$  is located within the gap,<sup>3,4</sup> but the gap formation mechanism is similar to that in the metallic case. In any case, the gap in the total DOS is an *indirect gap*, as sketched in Fig. 4(a), with the magnitude  $\Delta_{ind} \sim k_B T_K$ . Optical transitions across  $\Delta_{ind}$  are not allowed at low  $T$ 's due to the  $k$  conservation rule.<sup>20</sup> However, those across the *direct gap*,  $\Delta_{dir}$ , can occur as sketched in Fig. 4(a), resulting in a peak at  $\omega = \Delta_{dir}$  in  $\sigma(\omega)$ , shown in Fig. 4(b). In fact the mIR peaks observed for HF/IV compounds have been commonly interpreted as arising from such transitions.<sup>5,24</sup> The lack in the experimental  $\sigma(\omega)$  of a step-like onset at  $\Delta_{dir}$  sketched in Fig. 4(b) has been attributed to spectral broadening due to, e.g., impurities.

Clearly, the above model explains well the narrow Drude peak and the  $\tau^{-1} \propto \omega^2$  dependence of  $\text{YbAl}_3$  in this work. Regarding the mIR peak and the pseudogap of  $\text{YbAl}_3$ , however, the above theory cannot be applied directly since it predicts only a single peak away from  $\omega=0$  [Fig. 4(b)]. We attribute the mIR peak to optical transitions across  $\Delta_{dir}$  and the pseudogap to *indirect transitions across  $\Delta_{ind}$* . Although such indirect transitions are forbidden by the  $k$ -conservation rule as mentioned above, lattice disorder such as impurities may cause a partial relaxation of the rule, leading to indirect transitions. In addition, it has been pointed out<sup>4,29</sup> that many-body

scatterings, inherent in strongly-correlated systems, may provide the extra momentum needed for indirect transition. This would cause a long tail of  $\sigma(\omega)$  down to  $\Delta_{ind}$  as sketched in Fig 4(c), which is very similar to that observed for YbAl<sub>3</sub>. Our interpretation above is consistent with the following key experimental results and the theoretical predictions by the PAM: (i)The pseudogap width agrees well with  $T_K$  of YbAl<sub>3</sub>,  $\sim 60$  meV.<sup>15,18</sup> This is quite a strong evidence that the pseudogap is related with  $\Delta_{ind}$ . (ii)The mIR peak is centered at  $\sim 0.25$  eV, much larger than the pseudogap width. Theories<sup>26-29</sup> show that  $\Delta_{dir}$  can be several times larger than  $\Delta_{ind}$ , which is also seen from Fig. 4(a). The observed energies of the mIR peak and the pseudogap for YbAl<sub>3</sub> (0.25 eV/60 meV) is well within this range. (iii)The pseudogap disappears above 120 K, but the mIR peak is observed even at 690 K. In the theoretical  $\sigma(\omega)$ , although the gap is fully developed only at  $T \ll T_K$ , the spectral weight below  $\sim \Delta_{dir}$  begins to decrease at  $\sim T_K$ , as sketched in Fig. 4(d).<sup>26-28</sup>  $T_K$  of YbAl<sub>3</sub> is  $\sim 700$  K,<sup>15,18</sup> hence the observation of mIR peak up to 690 K is reasonable. Degiorgi *et al.*<sup>24</sup> have also argued that the mIR peaks observed for HF metals should correspond to  $\Delta_{dir}$ , and that their presence at  $T \gg T^*$  is reasonable, based on considerations on the PAM somewhat different from those in the present work.

We have shown that the observation of both a pseudogap and a mIR peak with different characteristic temperatures can be qualitatively explained by our model, taking into account the indirect transitions. However, some questions remain unanswered: At first, the theories<sup>4,29</sup> predict only a tail in  $\sigma(\omega)$ , as sketched in Fig. 4(c), decreasing from  $\omega = \Delta_{dir}$  to vanish at  $\Delta_{ind}$ . Namely, *these theories cannot account for the presence of a shoulder*; its microscopic origin remains unclear at the present time. It may be necessary to consider effects not included in the simple PAM, such as the orbital degeneracy, the crystal field, and the underlying band structure. In the case of Kondo semiconductor, a realistic theory including these effects has recently been started,<sup>31</sup> to understand the gap formation more consistently. Secondly, the band picture sketched in Fig. 4(a) is well defined only at  $T \leq T^*$ . At  $T \sim T_K$ , the quasiparticle lifetimes are too short to define such bands. The interpretation of mIR peak as “optical absorptions across  $\Delta_{dir}$ ” is invalid at high  $T$ . Presently, there seems no such clear-cut description for the mIR peak at high  $T$ . It probably results from a local charge excitation at each Yb site, but its microscopic character is unclear. Note that a simple excitation from a Kondo singlet is unlikely, since such excitation should involve a change in the spin and should be negligibly weak in  $\sigma(\omega)$ .<sup>20</sup> In addition, it is very remarkable that the inelastic neutron scattering experiment of YbAl<sub>3</sub> has revealed a pseudogap of about 30 meV at low temperatures.<sup>30</sup> The relation between the observed pseudogaps in the spin (neutron) and the charge (optical) excitation spectra is unclear. We expect that further advances in the theories of the  $f$ -electron systems should clarify these problems.

In conclusion, the  $\sigma(\omega)$  spectra of the IV compound YbAl<sub>3</sub> have been measured over wide ranges of  $\omega$  and

$T$ . They exhibited many characteristic features: an extremely narrow Drude peak, a pseudogap having a width of  $\sim k_B T_K$ , a pronounced mIR peak, and heavy-mass Fermi liquid properties. These features and their  $T$  dependences can be qualitatively understood based on PAM. In particular, the pseudogap and the mIR peak have been analyzed in terms of indirect and direct gaps within the PAM. To further establish the relation between the mIR peak/pseudogap and the  $c$ - $f$  hybridization, it will be useful to study  $\sigma(\omega)$  as a function of tunable hybridization strength. For this purpose, IR experiments on IV/HF compounds under hydrostatic pressure are under way.

## Acknowledgements

We thank T. Watanabe and M. Matsunami for technical assistance, and T. Mutou for many useful comments on the theoretical aspects. We also acknowledge useful discussions with H. Harima, J. Lawrence, J.-M. Mignot, P. Riseborough, and T. Saso. This work is partly supported by a Grant-in-Aid from MEXT. T.E. is financially supported by Yukawa Foundation and Corning Japan.

- 1) For recent development, see the papers in *International Conference on Strongly Correlated Electron Systems*, Acta Physica Polonica **34** (2003) 243-1634.
- 2) A.C. Hewson: *The Kondo Problem to Heavy Fermions* (Cambridge University Press, Cambridge, 1993).
- 3) G. Aeppli and Z. Fisk: Comments Condens. Matter Phys. **16** (1992) 155.
- 4) P.S. Riseborough: Adv. Phys. **49** (2000) 257.
- 5) Reviewed in L. Degiorgi: Rev. Mod. Phys. **72** (1999) 687.
- 6) B.C. Webb, A.J. Sievers and T. Mihalisin: Phys. Rev. Lett. **57** (1986) 1951.
- 7) P. Wachter and G. Travaglini: Phys. Rev. B **29** (1984) 893.
- 8) B. Bucher, Z. Schlesinger, P.C. Canfield and Z. Fisk: Phys. Rev. Lett. **72** (1994) 522.
- 9) H. Okamura, S. Kimura, H. Shinozaki, T. Nanba, F. Iga, N. Shimizu and T. Takabatake: Phys. Rev. B **58** (1998) R7496.
- 10) H. Okamura *et al.*: Phys. Rev. B **62** (2000) R13265.
- 11) S.V. Dordevic, D.N. Basov, N.R. Diley, E.D. Bauer and M.B. Maple: Phys. Rev. Lett. **86** (2001) 684.
- 12) M. Matsunami, H. Okamura, T. Nanba, H. Sugawara and H. Sato: J. Phys. Soc. Jpn. **72** (2003) 2722.
- 13) T. Ebihara *et al.*: Physica **B 281&282** (2000) 754.
- 14) T. Ebihara *et al.*: J. Phys. Soc. Jpn. **69** (2000) 895.
- 15) A.L. Cornelius *et al.*: Phys. Rev. Lett. **88** (2002) 117201.
- 16) T. Ebihara *et al.*: Phys. Rev. Lett. **90** (2003) 166404.
- 17) E.D. Bauer *et al.*: Phys. Rev. B **69** (2004) 125102.
- 18) S. Suga *et al.*: *Abstracts of the Fall Meeting, 2002* (Physical Society of Japan, 2002) 7aXC-6.
- 19) C. Homes, M.A. Reedyk, D.A. Crandels and T. Timusk: Appl. Opt. **32** (1993) 2976.
- 20) F. Wooten, *Optical Properties of Solids* (Academic Press, New York, 1972).
- 21) A preliminary part of this work appeared in H. Okamura, T. Ebihara and T. Nanba: Acta Physica Pol. B **34** (2003) 1075.  $\sigma(\omega)$  below 1 eV in this previous report was smaller than that in the present work, due to experimental errors.
- 22) A.V. Puchkov, D.N. Basov and T. Timusk: J. Phys. Condens. Matter **8** (1996) 10049.
- 23) N.W. Aschcroft and N.D. Mermin: *Solid State Physics* (Saunders College, Philadelphia, 1976).
- 24) L. Degiorgi, F.B.B. Anders and G. Gruner: Eur. Phys. J. B **19** (2001) 167.
- 25) A.J. Millis and P.A. Lee: Phys. Rev. B **35** (1987) 3394.
- 26) T. Mutou and D.S. Hirashima: J. Phys. Soc. Jpn. **63** (1994)

4475.

- 27) M. Jarrel: Phys. Rev. B **51** (1995) 7429.  
 28) M.J. Rozenberg, G. Kotliar and H. Kajueter: Phys. Rev. B **54** (1996) 8452.  
 29) N.S. Vidhyadhiraja, V.E. Smith, D.E. Logan and H.R. Krishnamurthy: J. Phys. Condens. Matter **15** (2003) 4045.  
 30) A.P. Murani: Phys. Rev. B **50** (1994) 9882.  
 31) T. Saso and H. Harima: J. Phys. Soc. Jpn. **72** (2003) 1131.

Fig. 1. (a) Optical reflectivity spectrum [ $R(\omega)$ ] of YbAl<sub>3</sub> at 295 K as a function of photon energy ( $\omega$ ). (b)  $R(\omega)$  of YbAl<sub>3</sub> between 8 and 690 K, and that of LuAl<sub>3</sub> at 295 K. The spectra of YbAl<sub>3</sub> above 295 K and that of LuAl<sub>3</sub> are measured above 0.06 eV only.

Fig. 2. (a)(b) Optical conductivity [ $\sigma(\omega)$ ] spectra of YbAl<sub>3</sub>. In (b) the vertical broken line and the vertical arrow indicate the shoulder and the pseudogap, respectively, as discussed in the text. (c)  $\sigma(\omega)$  at the pseudogap minimum at 27 meV (Pseudogap) and the intensity of the mIR peak integrated between 0.06 and 0.5 eV (mIR), normalized by those at 295 K, as a function of temperature ( $T$ ). (d) A comparison between the low-energy  $\sigma(\omega)$  and the dc conductivities, indicated at  $\omega=0$  with circle (8 K), square (80 K), triangle (160 K), and cross (295 K). The curves below 7 meV (the vertical broken line) are guide to the eye.

Fig. 3. (a) Energy-dependent scattering rate  $\tau^{-1}(\omega)$  of YbAl<sub>3</sub> as a function of the photon energy  $\omega$ . An  $\tau^{-1}(\omega) \propto \omega^2$  dependence is shown for comparison. (b) Energy-dependent effective mass  $m^*(\omega)$  relative to the bare optical mass  $m_b$ .

Fig. 4. Illustration of the theoretical predictions by the PAM discussed in the text. (a)  $c$ - $f$  hybridization states near the Fermi level ( $E_F$ ). The arrows indicate optical transitions across the direct ( $\Delta_{dir}$ ) and the indirect ( $\Delta_{ind}$ ) gaps. (b)  $\sigma(\omega)$  at  $T \ll T_K$  calculated with direct transitions only, and (c) that with both direct and indirect transitions. (d) Temperature dependence of  $\sigma(\omega)$ . Only direct transitions are included here.

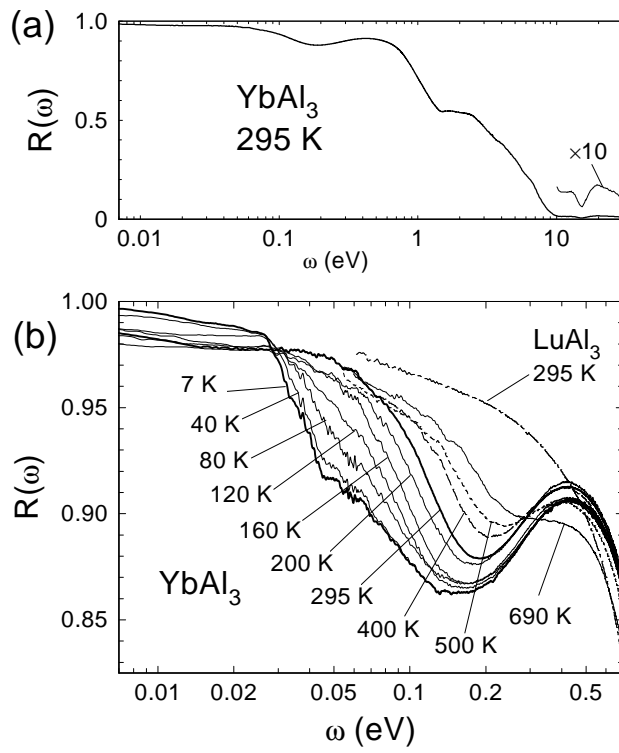


FIG. 1  
Okamura et al.

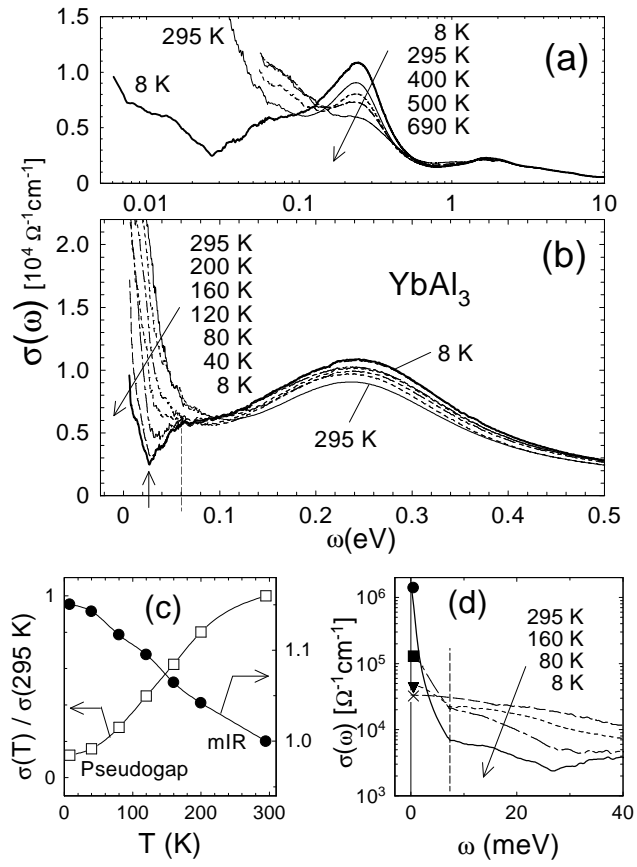


FIG. 2  
Okamura et al.

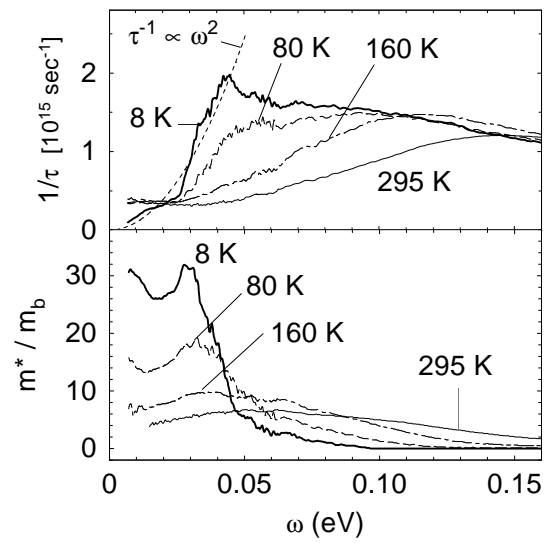


FIG. 3  
Okamura et al.

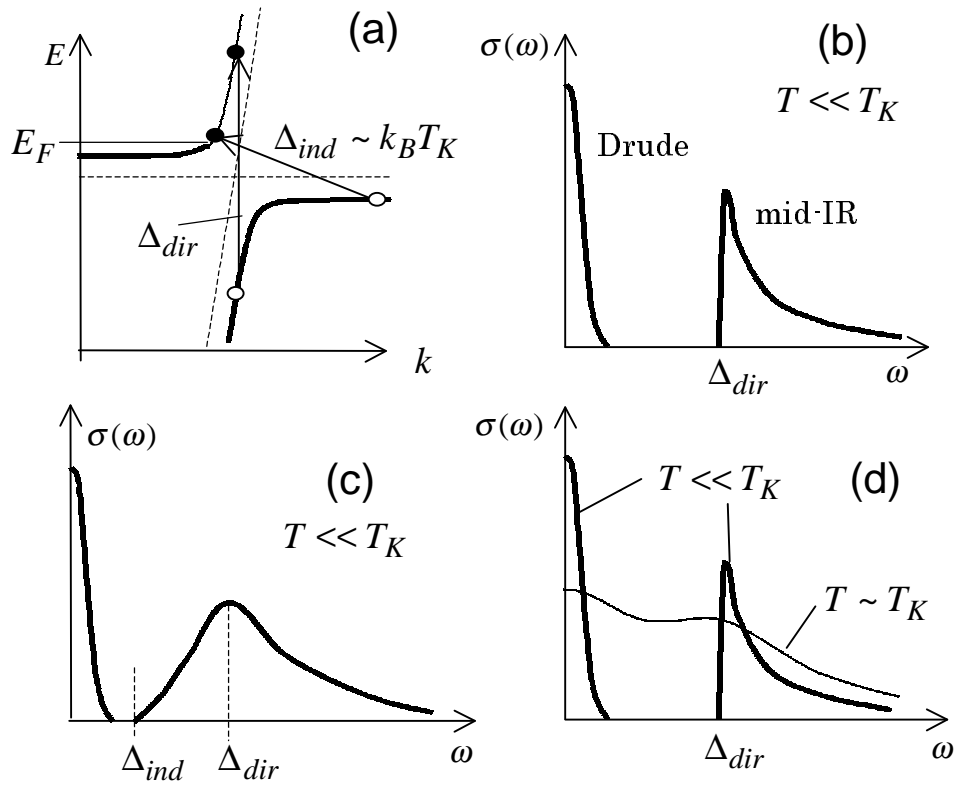


FIG.4

Okamura et al.